2.13 A COMPARISON OF LATENT HEAT FLUXES OVER GLOBAL OCEANS FOR FOUR FLUX PRODUCTS

Shu-Hsien Chou*
Department of Atmospheric Sciences, National Taiwan University, Taipei, Taiwan

Eric Nelkin, Joe Ardizzone, and Robert M. Atlas
Laboratory for Atmospheres, NASA/Goddard Space Flight Center, Maryland, USA

1. INTRODUCTION

To improve our understanding of global energy and water cycle variability, and to improve model simulations of climate variations, it is vital to have accurate latent heat fluxes (LHF) over global oceans. The LHF is derived using various bulk flux algorithms from surface winds, surface air humidity and temperature, and sea surface temperature, all of which may have a large uncertainty in the reanalyses, satellite retrievals, and in situ measurements. There is no "ground truth" for the global LHF fields; thus it is important to conduct intercomparison studies to assess the sources of errors for various global LHF products. The studies can identify the strengths and weaknesses of various LHF products, and provide important information for improving atmospheric general circulation models and satellite retrievals.

Currently, there are several datasets of global ocean LHF available, which are based on the surface air humidity and winds derived from the Special Sensor Microwave/Imager (SSM/I) on board a series of the Defense Meteorological Satellite Program (DMSP) spacecraft. The Hamburg Ocean Atmosphere Parameters and Fluxes from Satellite Data (HOAPS; Grassl et al. 2000) has daily and monthly LHF over global oceans with 0.5^o spatial resolution for the period July 1987–December 1998, based on the method of Schulz et al. (1997). The Goddard Satellite-based Surface Turbulent Fluxes (GSSTF) has two versions of global ocean LHF derived from the SSM/I radiances. The version 1 (GSSTF1) has daily and monthly fields for July 1987–December 1994 with a spatial resolution of 2.0^o x 2.5^o lat–lon (Chou et al. 1997, 2000). The version 2 (GSSTF2) has daily and monthly fields for July 1987–December 2000 with 1^o resolution (Chou et al. 2003). The Japanese Ocean Flux dataset with Use of Remote sensing Observations (J-OFURO) has monthly turbulent heat fluxes over global oceans with 1^o resolution for 1991–95 (Kubota et al., 2002). The J-OFURO has been further extended to the period 1992–2000 with 3 days temporal resolution. These flux datasets have been distributed to the SEAFLUX web site for intercomparison studies (Curry et al. 2004).

Kubota et al. (2003) compared the LHF of GSSTF1, HOAPS, J-OFURO, NCEP/NCAR reanalysis (Kalnay et al. 1996, referred to as NCEP), and the ECMWF (the European Centre for Medium–Range Weather Forecasts) analysis for 1992–94, as well as the LHF of da Silva et al. (1994, referred to as da Silva) for 1992–93, over the global oceans. Chou et al. (2003) compared the zonal averages of the GSSTF2 LHF and input parameters over global oceans with those of GSSTF1, HOAPS, NCEP, and da Silva for the 2yr-mean of 1992–93. Chou et al. (2004) have further improved the analysis for a detailed geographical comparison of the GSSTF2 LHF and input parameters with those of HOAPS, NCEP and da Silva over global oceans during 1992–93. In this paper, we present the major results of Chou et al. (2004).

2. DATA SOURCES

The basic data used in this study are 1^o x 1^o lat-lon monthly-mean latent heat fluxes, 10-m wind speed (U_{10m}), 10-m specific humidity (Q_{10m}), and sea-air humidity difference (Q_S–Q_{10m}) over global oceans for the period 1992–93 taken from GSSTF2, HOAPS, NCEP, and da Silva. These 1^o data are obtained from the 1^o data of GSSTF2 and da Silva, 1^o average of the 0.5^o data of HOAPS, and the Gaussian grid (~1.8^o) data of NCEP using bilinear interpolation. For proper comparison, the 2-m specific humidity of NCEP, and 20-m wind speed and 20-m specific humidity of da Silva are adjusted to 10-m height using the GSSTF2 bulk flux model. In addition, only the space and time matched 1^o monthly mean valid data for the common period of 1992–93 are used for the comparison.

To validate GSSTF2 daily LHF and input parameters, hourly measurements of surface meteorology and LHF of nine field experiments conducted by the NOAA/Environmental Technology Laboratory (ETL) research ships over the tropical and midlatitude oceans during 1991–99 are used (Fairall et al. 1997, 2003; Brunke et al. 2003; Chou et al. 2003). These nine experiments are the Atlantic Stratocumulus Transition Experiment (ASTEX), the Coupled Ocean-Atmosphere Response Experiment (COARE), the Fronts and Atlantic Storm Track Experiment (FASTEX), the Joint Air-Sea Monsoon Interaction Experiment

* Corresponding author adress: Dr. Shu-Hsien Chou, Dept. of Atmospheric Sciences, National Taiwan University, Taipei 106, Taiwan.
Email: shchou@atmos1.as.ntu.edu.tw

(JASMINE), the Kwajalein Experiment (KWAJEX), the Nauru '99 (NAURU99), the Tropical Instability Wave Experiment (TIWE), the Pan-American Climate Study in the eastern Pacific during 1999 (PACSF99), and the buoy service in the North Pacific (MOORINGS). The experiments provide hourly (50 min) covariance latent heat flux derived using the covariance or eddy correlation method.

3. VALIDATION OF GSSTF2 LHF

The daily-mean input parameters for calculating the GSSTF2 turbulent fluxes include SSM/I U_{10m} of Wentz (1997) and the Q_{10m}, which is derived from the SSM/I precipitable water of the entire atmospheric column and the 500-m layer near the surface (Chou et al. 1995, 1997). The input parameters also include the 2-m air temperature, SST, and sea level pressure of the NCEP/NCAR reanalysis (Kalnay et al. 1996). Using the GSSTF2 flux model, the GSSTF2 daily surface wind speed (U) and surface air specific humidity (Q_a) are adjusted to the measurement heights of the ships (~14–21 m) for proper validation. Compared to the nine experiments, Fig. 1 shows that, the GSSTF2 daily LHF has a bias of 0.8 W m^{-2}, a standard deviation (SD) error of 35.8 W m^{-2}, and a correlation of 0.83. The GSSTF2 daily wind speed has a bias of 0.36 m s^{-1}, a SD error of 1.38 m s^{-1}, and a correlation of 0.92. The GSSTF2 daily surface air specific humidity has a bias of 0.67 g kg^{-1}, a SD error of 1.23 g kg^{-1}, and a correlation of 0.97. The GSSTF2 daily SST has a negligible error.

Sources of retrieval-ship differences in daily LHF and input parameters include the spatial-temporal mismatch between GSSTF2 and ships, as well as the errors in the input parameters and fluxes for both GSSTF2 and ship observations. The collocated daily GSSTF2 variables are computed from 2–3 satellite observations averaged over a 1^o area that encloses the ship locations, while those of the ships are computed from at least two hourly measurements over a much smaller area. Daily retrieval errors may be assumed to be independent, as they are estimated from nine experiments covering different regions and time periods (not from a fixed location with continuous time periods). With this assumption, the SD errors reduce to 6.5 W m^{-2}, 0.25 m s^{-1}, and 0.22 g kg^{-1}, for the monthly-mean LHF, U, and Q_a, respectively.

4. COMPARISON OF RELEVANT PARAMETERS

The U_{10m} averaged over 1992–93 for GSSTF2, and the differences U_{10m}(HOAPS – GSSTF2), U_{10m}(NCEP – GSSTF2), and U_{10m}(da Silva – GSSTF2), respectively, for the 2-yr period over global oceans are shown in Fig. 2. Figure 2a shows that the maximum annual mean wind speed is located in the trade-wind belts (~8–9 m s^{-1}) and extratropical storm-track regions (~8–11 m s^{-1}). The minimum wind speed is located in the weak-wind (~4–6 m s^{-1}) areas of the equatorial Indian Ocean, South Pacific convergence zone (SPCZ), and intertropical convergence zone (ITCZ), and the subtropical highs (~7 m s^{-1}). Figure 2b shows that the HOAPS U_{10m} is significantly smaller than GSSTF2 in the tropical oceans with a difference up to 2 m s^{-1} centered near the locations of the maximum wind in the trade wind belts of both hemispheres. Over the extratropical oceans, on the contrary, the HOAPS U_{10m} is larger than GSSTF2 with a maximum difference of 2 and 1.5 m s^{-1}, centered near 50^oN and 50^oS, respectively.

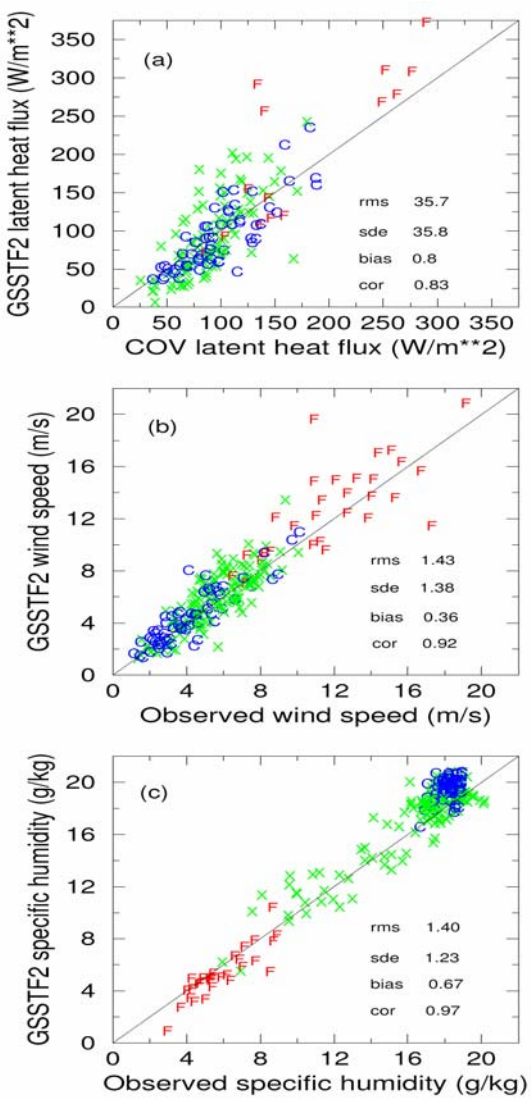

Fig. 1. GSSTF2 daily (a) latent heat fluxes, (b) surface winds, and (c) surface air specific humidity versus those of nine field experiments. C is for COARE, F for FASTEX, and X for other experiments.

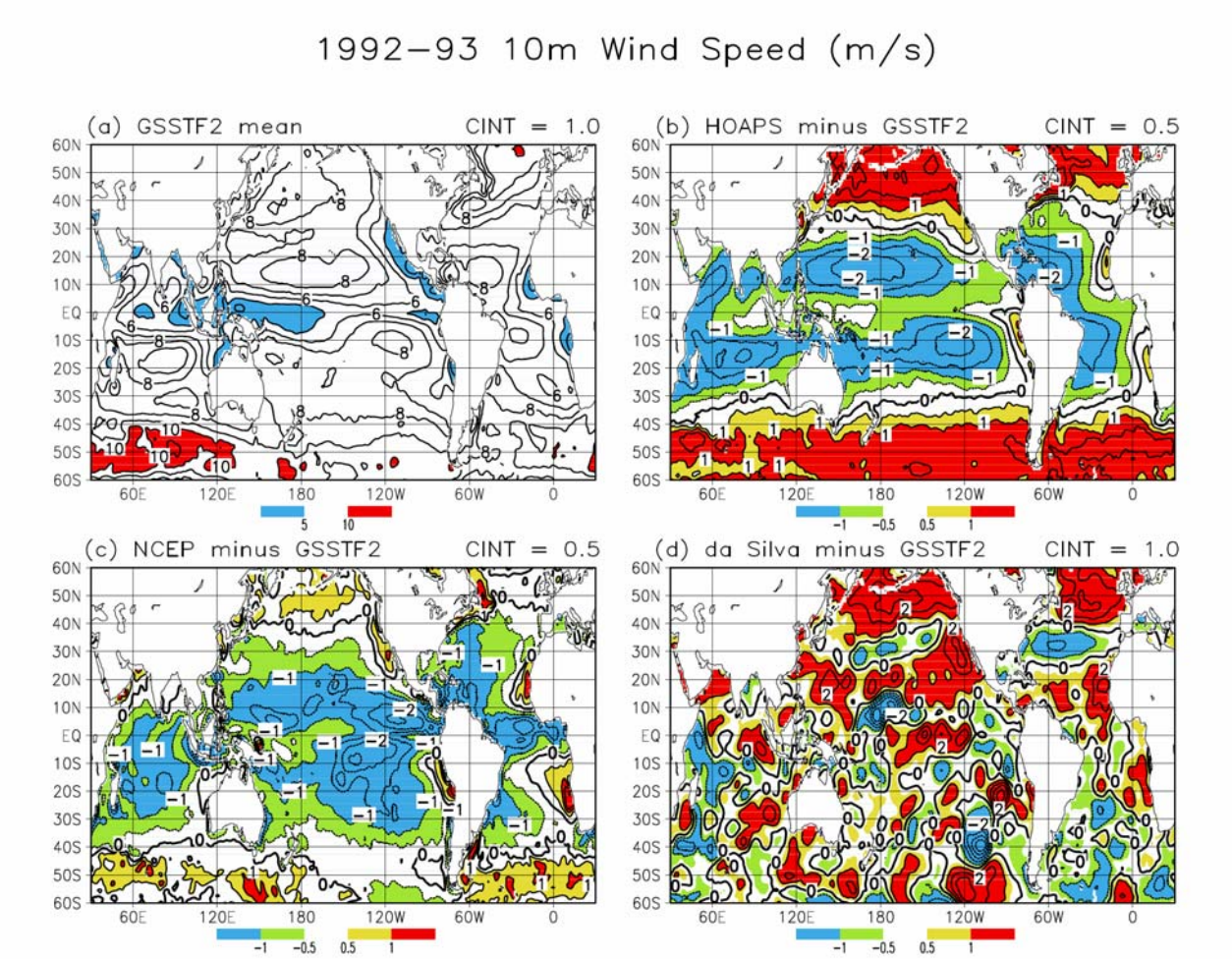

Fig. 2. The 10-m wind speed averaged over 1992–93 for (a) GSSTF2, and differences of (b) HOAPS, (c) NCEP, and (d) da Silva from GSSTF2. Only collocated monthly valid data from all four datasets are used.

Figure 2c shows that the NCEP U_{10m} is also significantly smaller than GSSTF2 in the tropics (equatorward of ~40^o, except the eastern boundary current regions in the Pacific and Atlantic), with the maximum difference of 2 m s^{-1} near the equator. Over the extratropics, the NCEP U_{10m} is larger than GSSTF2 with the maximum difference of 0.5 and 1 m s^{-1} around 50^{o}N and 50^{o}S, respectively. Figure 2d shows that U_{10m}(da Silva – GSSTF2) has small-scale features and is quite different from the large-scale patterns of U_{10m}(HOAPS – GSSTF2) and U_{10m}(NCEP – GSSTF2) shown in Figs. 2b and 2c. Over the oceans north of ~10^{o}N, U_{10m}(da Silva – GSSTF2) is generally positive in the high wind areas of the extratropical storm track regions and trade wind belts (by ~2–3 m s^{-1}), but is generally negative in the weak wind areas of the subtropical highs (by ~1–2 m s^{-1}). Over the oceans south of 10^{o}N, it characterizes the small-scale features with neighboring significant large positive and negative difference centers, especially with the magnitude of U_{10m} difference reaching ~4–5 m s^{-1} over the data-void region of the eastern South Pacific.

The Wentz (1997) SSM/I U_{10m} from 1987 to 1997 have been extensively evaluated with those of the Tropical Atmosphere-Ocean (TAO) and National Data Buoy Center (NDBC) buoys by Mears et al. (2001), and those of the ECMWF analysis and NCEP by Meissner et al. (2001). Meissner et al. (2001) pointed out that both global analyses did not assimilate the Wentz wind products and that the SSM/I wind speeds assimilated in NCEP were derived using a neural network algorithm and were different from those of Wentz (1997). Mears

et al. (2001) found that the mean difference between SSM/I and buoy winds was typically < 0.4 m s^{-1} and the SD error was <1.4 m s^{-1}. Meissner et al. (2001) found that the collocated SSM/I and NCEP U_{10m} had a SD difference of 2.4 m s^{-1}, which reduced to 1.2 m s^{-1} for the monthly averages, and that the NCEP U_{10m} was underestimated in the tropical Pacific and tropical Atlantic. Wang and McPhaden (2001) found the NCEP surface winds were weaker than those of TAO buoys by ~1–1.5 m s^{-1} in the equatorial Pacific. Smith et al. (2001) found the NCEP U_{10m} was underestimated by 0.4–1.0 m s^{-1} for five geographic regions (the North Atlantic, South Atlantic, Southern Ocean, Western Pacific, and Arabian Sea), as compared to those measured by research ships during the 1990–95 World Ocean Circulation Experiment. Renfrew et al. (2002) found that the NCEP U_{10m} was 0.4 m s^{-1} higher than those measured by the research ship over the Labrador Sea. Brunke et al. (2002) found that the HOAPS surface wind was underestimated by ~1 m s^{-1} during 1992-93 as compared to those measured by TAO buoys in the equatorial Pacific. These results and Kubota et al. (2003) are consistent with this study.

Da Silva et al. (1994) assumed an anemometer height of 20 m to the entire wind dataset measured by ship anemometers of the Comprehensive Ocean-Atmosphere Data Set (COADS) to derive a Beaufort equivalent scale for determining visual wind speeds, which depend on sea states. However, Kent and Taylor (1997) found that the true anemometer heights had large standard deviations with the means generally much higher than 20 m and increasing with time. For example, they found that the mean anemometer height was 35.2 m (24.2 m) with a standard deviation of 8.4 m (10.9 m) in middle latitudes of the North Pacific (North Atlantic) during 1990. An underestimation of anemometer height can cause unrealistic higher ship anemometer-measured (and visual) wind speeds, because the higher wind speeds measured at the higher anemometer heights are assigned to the assumed lower levels. For the same error of anemometer height, the stronger the wind is, the larger the wind speed error is. This can cause a larger discrepancy of wind speeds in the high-wind regions. This is likely to be the major reason that a large discrepancy of U_{10m} in the high-wind region of the Northern Hemisphere is found between da Silva and GSSTF2. Figure 1b suggests that the GSSTF2 monthly wind speed has a bias of 0.36 m s^{-1}, and a SD error of 0.25 m s^{-1}, respectively. This result and the above mentioned previous studies suggest that the GSSTF2 U_{10m} is more accurate and that the differences (Fig. 2) are most likely mainly caused by the errors in HOAPS, NCEP, and da Silva.

Figure 3 shows the Q_{10m} averaged over 1992–93 for GSSTF2, and the differences Q_{10m}(HOAPS – GSSTF2), Q_{10m}(NCEP – GSSTF2), and Q_{10m}(da Silva – GSSTF2), respectively, over global oceans. Figure 3a shows that the Q_{10m} has a maximum of >18 g kg^{-1} in the equatorial warm pool and decreases poleward, with the pattern similar to that of SST. The large-scale patterns of Q_{10m} for HOAPS, NCEP, and da Silva averaged over 1992-93 (not shown) are similar to that of GSSTF2. However, Figs. 3b–3d show significant differences with GSSTF2. Figure 3b shows that the HOAPS Q_{10m} is higher than GSSTF2 over the global oceans with the maximum difference of 1.0–1.5 g kg^{-1} in the tropics with high SST. The minimum Q_{10m} difference of <~0.5 g kg^{-1} is located in the areas poleward of ~50^o, as well as the dry tongue regions of the eastern South Pacific and Atlantic.

Figure 3c shows that, over the equatorial Indian Ocean, SPCZ, and ITCZ, the NCEP Q_{10m} is smaller than GSSTF2 by ~0.5–1.0 g kg^{-1}, while it is significantly larger than GSSTF2 by ~0.5–2.5 g kg^{-1} for the rest of the global oceans. The maximum difference in Q_{10m} is ~2.5 g kg^{-1} in the trade wind and dry tongue area of the eastern South Pacific, ~2 g kg^{-1} in the other trade wind areas and ~1 g kg^{-1} in the extratropical oceans. We note that the dry tongue of the HOAPS Q_{10m} is similar to that of GSSTF2 over the eastern South Pacific, but the dry tongue of NCEP is significantly weaker than that of GSSTF2 (not shown). This result can be inferred from Figs. 3b and 3c. Figure 3d shows that Q_{10m}(da Silva – GSSTF2) is characterized by small-scale features with large magnitudes of differences over data sparse regions, especially the equatorial Pacific and oceans south of ~30^oS. The large-scale pattern of Q_{10m}(da Silva – GSSTF2) (Fig. 3d) is similar to that of Q_{10m}(NCEP – GSSTF2) (Fig. 3c) north of ~25^oS but is quite different south of 25^oS. This is because the same observed surface air humidity data of COADS were used in both NCEP and da Silva.

The Q_{10m} of da Silva undulates in the zonal direction (which is very different from the large-scale and smoothing patterns of other three data sets) and does not follow the SST pattern south of ~30^oS (not shown). Thus there are significant smaller scale differences in the zonal belt of 30^oS–50^oS (Fig. 3d). In addition, the Q_{10m} of da Silva is generally lower than GSSTF2 in the equatorial areas (where the Q_{10m} is the highest) but is generally higher than GSSTF2 poleward of these regions. Compared to GSSTF2, the da Silva Q_{10m} thus has smaller poleward gradient, which is an indication of a smoothing effect from the successive corrections of da Silva. The positive differences are especially large south of 30^oS. Since data are scarce in the oceans south of 30^oS, the high Q_{10m} (and SST) observed further equatorward is extrapolated poleward (Kent et al. 2000). This can cause da Silva to have unrealistic high values of Q_{10m} (and SST) south of 30^oS and to have large differences with GSSTF2 there (Figs. 3d and 4d).

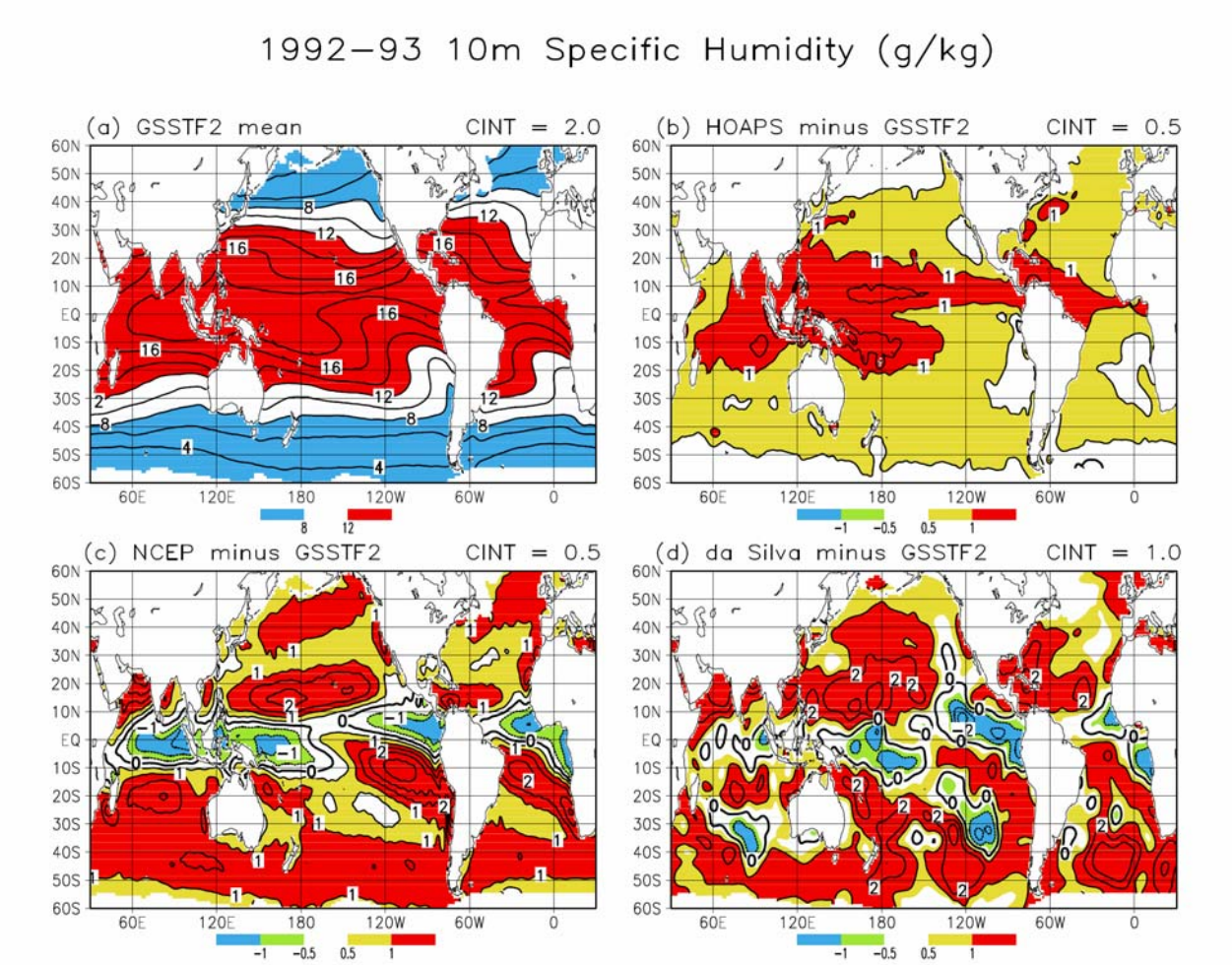

Fig. 3. Same as Fig. 2, except for 10-m specific humidity.

Figure 1c shows that the GSSTF2 Q_a has a positive bias for the moist region with Q_a of ~16–20 g kg^{-1} but has a small negative bias for the dry region with Q_a of ~3–6 g kg^{-1}. Thus Figs. 1c, 3a, and Fig. 3b suggest that the HOAPS Q_{10m} is significantly overestimated in the tropical oceans, as it is larger than the moist biased Q_a of GSSTF2. This result indicates that the positive bias of J-OFURO Q_{10m} is also larger than that of GSSTF2 in the tropical oceans, as the same humidity retrieval technique as HOAPS is used. In addition, Wang and McPhaden (2001), Smith et al. (2001), and Renfrew et al. (2002) found that the NCEP surface air humidity had positive biases when compared with those measured by TAO buoys and research ships. Their results and this study imply that the positive Q_{10m}(NCEP – GSSTF2) shown in Fig. 3c is mostly a result of the moist bias of NCEP, while the negative Q_{10m}(NCEP – GSSTF2) is likely mostly due to the moist bias of GSSTF2. Previous studies (e.g., da Silva et al. 1994; Chou et al. 1997; Josey et al. 1999) found that ship observations overestimated dew point temperatures (by ~0.5^{o}C), which resulted in moist bias of the surface air humidity for COADS, and thus for da Silva and NCEP. Their results and this study suggest that the moist bias of da Silva is likely responsible for the positive Q_{10m}(da Silva – GSSTF2) shown in Fig. 3d. These analyses suggest that the GSSTF2 Q_{10m} is likely to have better quality than the other three datasets analyzed, although it is still subject to regional biases.

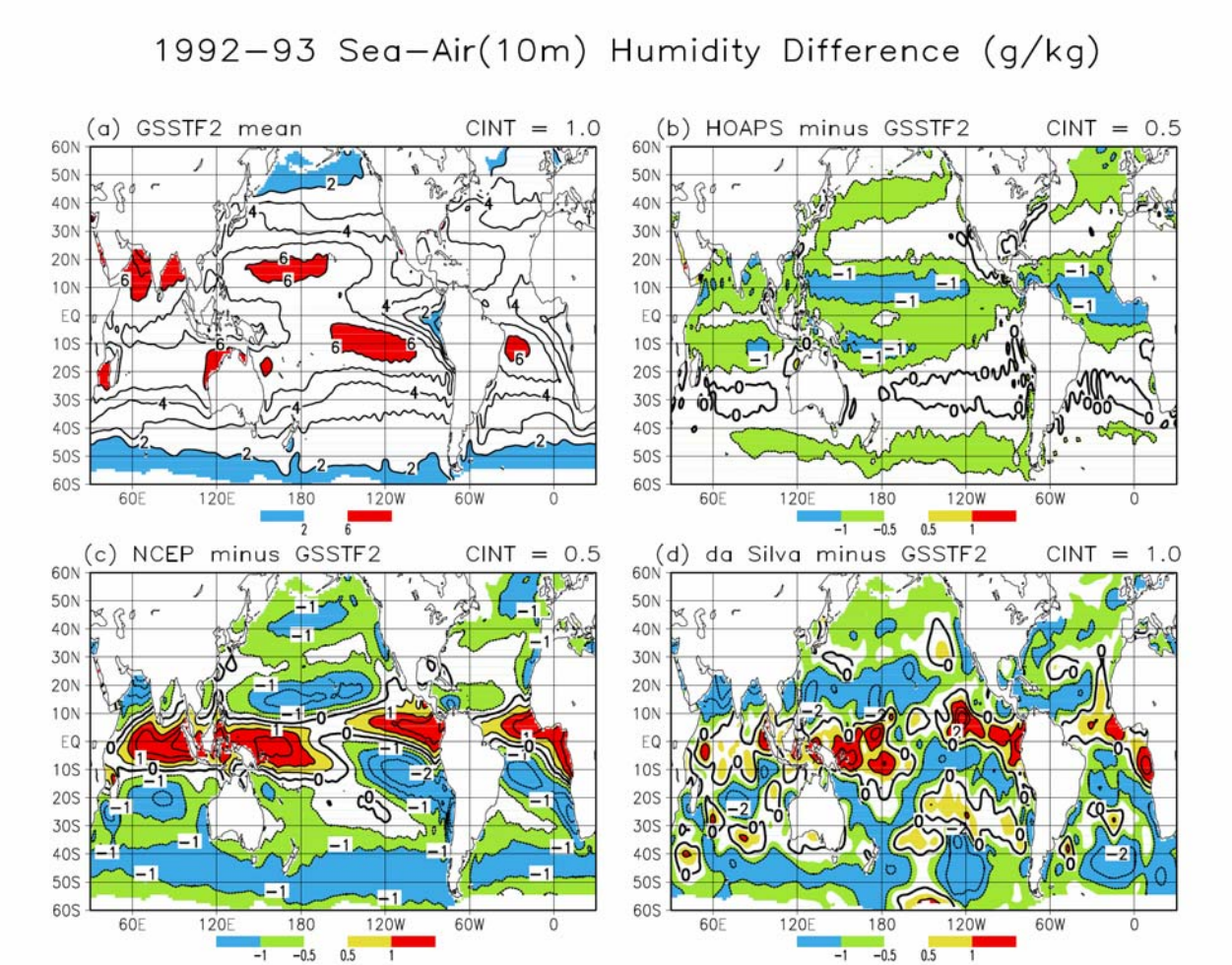

Fig. 4. Same as Fig. 2, except for sea–10m humidity differences.

Figure 4 shows the Q_S–Q_{10m} averaged over 1992–93 for GSSTF2, and the differences [(Q_S–Q_{10m})(HOAPS – GSSTF2)], [(Q_S–Q_{10m})(NCEP – GSSTF2)], and [(Q_S–Q_{10m})(da Silva – GSSTF2)], respectively, over global oceans. It is noted that there is a 2% reduction in calculating Q_S due to salinity effect in GSSTF2, HOAPS, and da Silva, but not in NCEP. In addition, due to the use of the approximate formulation (0.622 e/P), instead of the exact formula [0.622 e/(P-0.378e)], there is a partial cool skin effect on the GSSTF2 Q_S (Chou et al. 2003). Figure 4a shows that the Q_S–Q_{10m} has maximum values of ~6 g kg^{-1} over the trade wind belts of both hemispheres and decreases to <~2 g kg^{-1} poleward of ~50^o resulting from the reduction of SST. Over the equatorial region (10^{o}S–10^{o}N), the Q_S–Q_{10m} has a large value of ~5 g kg^{-1} in the high SST regions of the Indian Ocean and western Pacific, and decreases eastward in the eastern Pacific due to upwelling-induced decrease in the SST. Figure 4b shows that the HOAPS Q_S–Q_{10m} is smaller than GSSTF2 by ~0.5–1 and 0–0.5 g kg^{-1}, respectively, in the areas equatorward and poleward of ~20^o. This is consistent with the finding of Brunke et al. (2002) that the HOAPS sea-air humidity difference was underestimated by ~0.5–1 g kg^{-1} during 1992-93 as compared to those measured by TAO buoys in the equatorial Pacific. The difference in Q_S–Q_{10m} is smaller over the dry or cold tongue areas of the eastern South Pacific and South Atlantic, with the minimum difference ~30^{o}S.

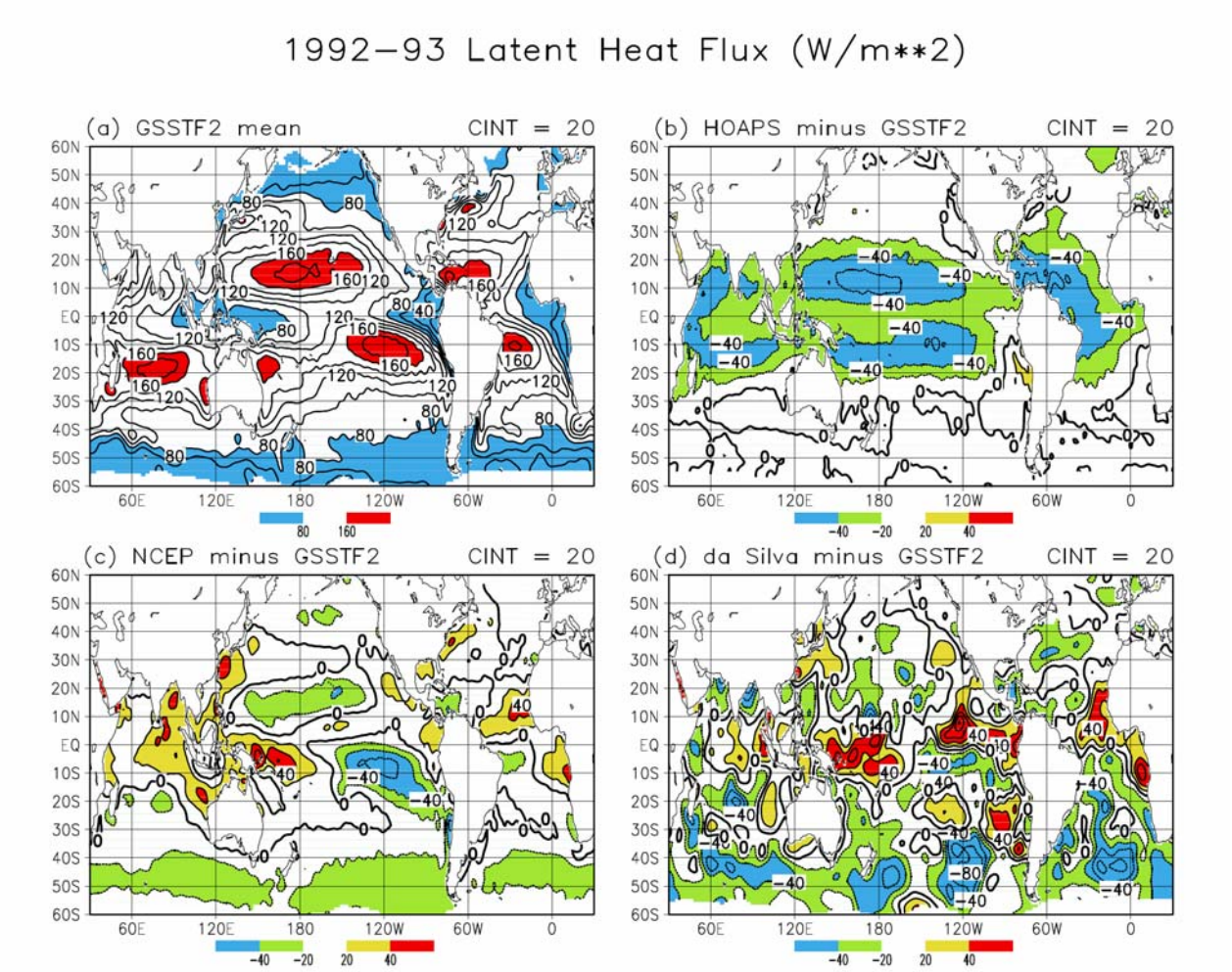

Fig. 5. Same as Fig. 2, except for latent heat fluxes.

Figure 4c shows that, over the regions of the equatorial Indian Ocean, SPCZ, and ITCZ, the NCEP Q_S–Q_{10m} is significantly larger than GSSTF2 by ~0.5–1.5 g kg^{-1}. For the rest of the global oceans, it is significantly smaller than GSSTF2 by ~0.5–2.0 g kg^{-1}, with the maximum difference reaching ~2 g kg^{-1} over the trade wind area in the eastern South Pacific, up to ~1.5 g kg^{-1} in the other trade wind areas, and ~1 g kg^{-1} in the extratropical oceans. Figure 4d shows that the [(Q_S–Q_{10m})(da Silva – GSSTF2)] has small-scale structures with large magnitudes of differences over data sparse regions, especially the equatorial Pacific and the oceans south of 30°S. The large-scale pattern of [(Q_S–Q_{10m})(da Silva – GSSTF2)] (Fig. 4d) is similar to that of [(Q_S–Q_{10m})(NCEP – GSSTF2)] (Fig. 4c) north of ~25°S but is quite different south of 25°S. It can be seen from Figs. 3 and 4 that, for these datasets, the differences in Q_{10m} mainly control the differences in Q_S–Q_{10m} and the differences in Q_S are relatively small (see Table 1), which is consistent with the results of Chou et al. (2003).

5. COMPARISON OF LHF

The LHF averaged over 1992–93 for GSSTF2, and the differences LHF(HOAPS – GSSTF2), LHF(NCEP – GSSTF2), and LHF(da Silva – GSSTF2), respectively, for the 2-yr period over global oceans are shown in Fig. 5. Figure 5a shows that the maximum LHF is located in the trade wind belts of both hemispheres (~160–180 W m^{-2}) and in the western boundary current regions of the Kuroshio and Gulf Stream (~160 W m^{-2}). This results from high winds (~8–9 m s^{-1}) coupling with large Q_S–Q_{10m} (~5–6 g kg^{-1}) in these areas (Figs. 2a and 4a). The minimum LHF (<~60 W m^{-2}) is found in the eastern equatorial Pacific and Atlantic, due to upwelling-induced cold SSTs associated with weak winds, and in the high

latitudes due to poleward decrease of SST. We note that the general patterns of U_{10m}, Q_S–Q_{10m}, and LHF of GSSTF2 for 1992–93 (Figs. 2a, 4a, and 5a) are similar to those of Chou et al. (2003) for 1988–2000. For the 1992–93 mean condition, the large-scale pattern of the GSSTF2 LHF shown in Fig. 5a is similar to those of HOAPS, NCEP, and da Silva (not shown). However, there are significant differences with GSSTF2 geographically.

The LHF is computed using the aerodynamic bulk method with stability dependency for all four flux products. The stability-dependent transfer coefficient for moisture is determined based on the surface layer similarity theory. The coefficients of HOAPS and da Silva are based on Smith (1988) and Large and Pond (1982), respectively. Both coefficients are very close to that of GSSTF2 (Brunke et al. 2003). Thus, the discrepancy in the LHF among GSSTF2, HOAPS, and da Silva is primarily caused by the differences in the input parameters. However, this situation is not true for NCEP. The moisture transfer coefficient of NCEP is significantly larger than that of GSSTF2 (and the other two flux datasets; Zeng et al. 1998), which appears to offset the effects of weaker winds and smaller sea-air humidity difference on the LHF (Figs. 2c and 4c).

Figure 5b shows that the HOAPS LHF is significantly smaller than that of GSSTF2 over the global oceans, especially in the tropics. In the tropical oceans, the difference is ~20–60 W m^{-2}, with the maximum differences of ~60 and 40 W m^{-2} centered ~10^{o}N and 10^{o}S, respectively. The difference decreases poleward and is negligible south of ~30^{o}S. In the tropical oceans, the negative LHF(HOAPS – GSSTF2) is a result of smaller U_{10m} and Q_S–Q_{10m} of HOAPS (Figs. 2b and 4b). For the negative LHF(HOAPS – GSSTF2) in the oceans north of 30^{o}N, the effect of the smaller HOAPS Q_S–Q_{10m} (coupling with high winds) slightly overcompensates the effect of higher U_{10m} (coupling with low Q_S–Q_{10m}) on the LHF. For the negligible LHF difference in the oceans south of ~30^{o}S, the effects of smaller Q_S–Q_{10m} and larger U_{10m} on LHF generally offset each other. Note that Brunke et al. (2002) found that the HOAPS LHF was underestimated by ~30 W m^{-2} during 1992-93 as compared to those derived from the TAO buoy measurements in the equatorial Pacific. Their result is consistent with our study.

Figure 5c shows that the NCEP LHF is larger than GSSTF2 in the equatorial Indian Ocean, SPCZ, ITCZ, the Kuroshio and Gulf Stream, and subtropics, with the maximum difference up to 40 W m^{-2}. For the rest of the global oceans, the NCEP LHF is smaller than GSSTF2, with the maximum difference of ~60 W m^{-2} located in the dry tongue and trade wind region of the eastern South Pacific. For the trade wind regions (especially over the South Pacific dry tongue), the negative LHF(NCEP – GSSTF2) is a result of smaller U_{10m} and Q_S–Q_{10m} of NCEP (Figs. 2c and 4c). The positive LHF(NCEP – GSSTF2) in the equatorial Indian Ocean, SPCZ, and ITCZ is due to the effects of larger NCEP Q_S–Q_{10m} and moisture transfer coefficient overcompensating the effect of smaller U_{10m} on the LHF. The negative LHF(NCEP – GSSTF2) in the extratropical oceans is due to the effect of smaller NCEP Q_S–Q_{10m} overcompensating the effects of larger U_{10m} and moisture transfer coefficient on the LHF.

Figure 5d shows the LHF(da Silva – GSSTF2) has small-scale structures, with its large-scale pattern somewhat similar to that of LHF(NCEP – GSSTF2) (Fig. 5c). For example, the da Silva LHF is larger than GSSTF2 in the equatorial Indian Ocean, SPCZ, ITCZ, and the Kuroshio area, but with a larger difference of 20–60 W m^{-2}. In addition, the da Silva LHF is smaller than GSSTF2 in the trade wind regions and the oceans south of 30^{o}S, but with significantly larger localized differences of 20–80 W m^{-2}. Note that Fig. 5d shows that there are some neighboring extreme large positive and negative difference centers of LHF located in the data sparse regions for da Silva. This feature is quite different than the more organized large-scale patterns of LHF difference for HOAPS and NCEP (Figs. 5b and 5c), which was also found in Kubota et al. (2003).

Figure 6 shows the SD of difference (SDD) and temporal cross correlation of monthly LHF between GSSTF2 and each of HOAPS, NCEP, and da Silva, respectively, during 1992–93 over global oceans. Figure 6a and 6b show that the SDD in LHF is generally ~10–20 W m^{-2} over the oceans, with a high correlation of 0.8–0.9 (0.6–0.8) in the oceans north of ~20^{o}S (south of 20^{o}S). This implies that the monthly LHF(HOAPS – GSSTF2) has a relatively smaller temporal variability in the oceans north of 20^{o}S than the oceans south of 20^{o}S. Figure 6c and 6d show that, over the tropical oceans, the SDD in LHF has a large value of ~20–30 W m^{-2} with a low correlation of 0.6–0.9 (0.3–0.6 in the ITCZ), which implies that the monthly LHF (NCEP – GSSTF2) has a large temporal variability there, especially over the ITCZ. In the extratropical oceans, the SDD in LHF reduces to ~10–20 W m^{-2} with an increased correlation of 0.8–0.9 (larger for the northern than the southern extratropical oceans). This implies that the monthly LHF (NCEP – GSSTF2) has a smaller temporal variability in the extratropical oceans than in the tropical oceans. Figure 6e and 6f show that the SDD in LHF generally has a large value of ~20–40 W m^{-2} over most of the global oceans, with the correlation of <0.6 over most of the areas south of ~30^{o}N. This implies that the monthly LHF(da Silva – GSSTF2) has a large temporal variability over most of the oceans, especially the equatorial and southern extratropical oceans.

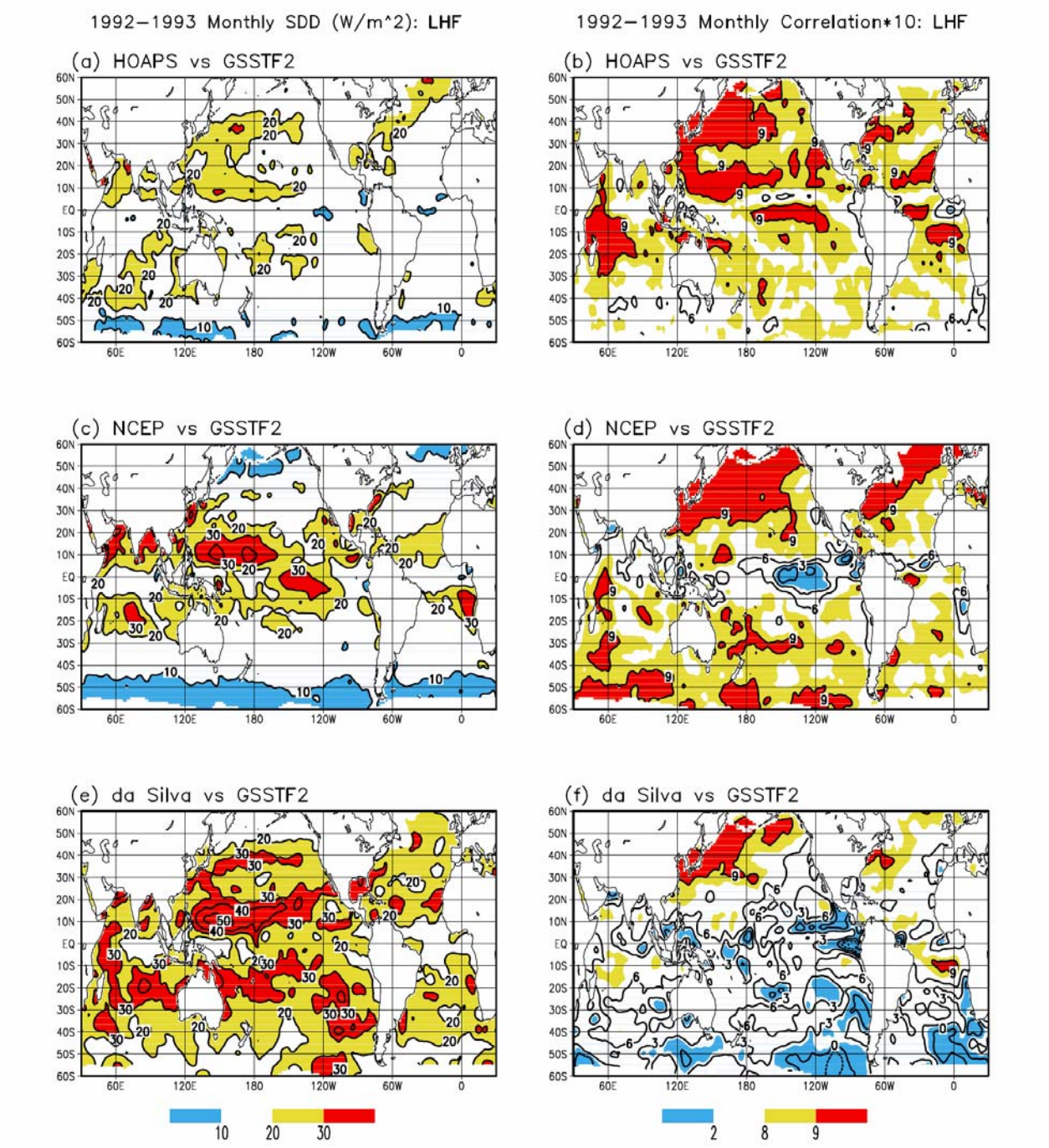

Fig. 6. Standard deviations of differences (left) and temporal cross correlation (right) of monthly latent heat fluxes between GSSTF2 and each of (a, b) HOAPS, (c, d) NCEP, and (e, f) da Silva during 1992–93.

Table 1. Regional-mean LHF, U_{10m}, Q_s–Q_{10m}, Q_{10m}, and Q_s over global oceans during 1992–93 for GSSTF2, as well as the differences of HOAPS, NCEP, and da Silva from GSSTF2.

Variable	Source	60°S–60°N	20°N–60°N	20°S–20°N	20°S–60°S
LHF	GSSTF2	108.2	104.1	122.1	94.3
(W m^{-2})	HOAPS	–19.7	–14.3	–37.4	–2.0
	NCEP	–3.4	+0.5	+3.0	–13.2
	Da Silva	–8.5	–5.3	+1.3	–21.8
U_{10m}	GSSTF2	7.39	7.33	6.63	8.25
(m s^{-1})	HOAPS	–0.26	+0.22	–1.13	+0.45
	NCEP	–0.59	–0.27	–1.04	–0.26
	Da Silva	+0.30	+0.84	+0.27	+0.04
Q_s–Q_{10m}	GSSTF2	4.14	3.80	5.10	3.20
(g kg^{-1})	HOAPS	–0.48	–0.43	–0.70	–0.23
	NCEP	–0.51	–0.67	–0.09	–0.92
	Da Silva	–0.53	–0.70	–0.27	–0.74
Q_{10m}	GSSTF2	12.07	10.19	16.63	7.81
(g kg^{-1})	HOAPS	+0.83	+0.71	+1.07	+0.59
	NCEP	+0.85	+0.95	+0.53	+1.14
	Da Silva	+0.95	+1.14	+0.67	+1.15
Q_S	GSSTF2	16.22	14.01	21.73	11.01
(g kg^{-1})	HOAPS	+0.35	+0.28	+0.37	+0.36
	NCEP	+0.33	+0.29	+0.44	+0.22
	Da Silva	+0.41	+0.44	+0.44	+0.41

Table 2. Regional-mean std dev of differences/temporal cross correlation of monthly LHF, U_{10m}, Q_s–Q_{10m} and Q_{10m} between GSSTF2 and each of HOAPS, NCEP, and da Silva over global oceans during 1992–93.

Variable	Source	60°S–60°N	20°N–60°N	20°S–20°N	20°S–60°S
LHF	HOAPS	16.8/0.81	18.9/0.87	16.9/0.83	15.6/0.77
(W m^{-2})	NCEP	18.3/0.78	17.4/0.88	23.0/ 0.69	13.4/0.84
	Da Silva	25.7/0.51	25.1/0.73	27.0/0.54	24.4/0.35
U_{10m}	HOAPS	0.67/0.85	0.79/0.87	0.61/0.87	0.67/0.81
(m s^{-1})	NCEP	0.63/0.84	0.59/0.91	0.71/0.80	0.56/0.86
	Da Silva	1.01/0.55	0.98/0.71	0.93/0.64	1.12/0.35
Q_s–Q_{10m}	HOAPS	0.52/0.77	0.57/0.81	0.55/0.81	0.45/0.70
(g kg^{-1})	NCEP	0.71/0.50	0.69/0.70	0.93/0.27	0.47/0.66
	Da Silva	0.75/0.34	0.78/0.59	0.80/0.31	0.67/0.24
Q_{10m}	HOAPS	0.38/0.97	0.48/0.98	0.37/0.97	0.35/0.96
(g kg^{-1})	NCEP	0.70/0.85	0.67/0.96	0.92/0.71	0.46/0.95
	Da Silva	0.83/0.81	0.82/0.94	0.88/0.78	0.77/0.79

Table 1 shows the regional averages of LHF and input parameters for the global oceans (60°S–60°N), northern extratropical oceans (20°N–60°N), tropical oceans (20°S–20°N), and southern extratropical oceans (20°S–60°S) during 1992–93 for GSSTF2, as well as the differences of HOAPS, NCEP, and da Silva from GSSTF2. The global-mean LHF is the largest for GSSTF2 (108.2 W m^{-2}) and is the smallest for HOAPS (88.5 W m^{-2}), with a difference of 20 W m^{-2}. Over the tropical oceans, the HOAPS LHF is significantly smaller than GSSTF2 by ~31% (37 W m^{-2}), whereas the other two datasets are comparable to GSSTF2. This is because the HOAPS LHF is systematically smaller than GSSTF2 in space, while the other two datasets have very large spatial variations in LHF with large positive and negative differences, which cancel to produce

smaller regional-mean differences (Fig. 5). The smallness of HOAPS LHF in the tropical oceans is mainly a result of weaker U_{10m} (by ~1.1 m s^{-1}) coupling with smaller Q_S–Q_{10m} (by ~0.7 g kg^{-1}). The significant larger Q_{10m} (by 1.1 g kg^{-1}) is the main cause for the smallness of HOAPS Q_S–Q_{10m}.

The global-mean LHF of NCEP is comparable to that of GSSTF2, but U_{10m} and Q_S–Q_{10m} are smaller (by ~0.6 m s^{-1} and ~0.5 g kg^{-1}), which appear to offset the larger moisture transfer coefficient (Zeng et al. 1998). Due to the cancellation of large local positive and negative differences with GSSTF2, the regional-mean LHF of da Silva appears to be comparable to that of GSSTF2, except for the southern extratropical oceans. Over the southern extratropics, the da Silva LHF is the smallest among the four datasets (Fig. 5 and Table 1), ~23% (22 W m^{-2}) smaller than GSSTF2. This discrepancy is mainly due to a larger Q_{10m} (by ~1.2 g kg^{-1}) and is most likely due to the errors arising from extrapolating high values of Q_{10m} from low latitudes to the large data-void regions in the southern extratropical oceans as discussed before (see Fig. 3d).

Table 2 shows regional-mean standard deviation of differences/temporal cross correlation of monthly LHF and input parameters for the global oceans, northern extratropical oceans, tropical oceans, and southern extratropical oceans between GSSTF2 and each of HOAPS, NCEP, and da Silva during 1992–93. Averaged over the global oceans, HOAPS has the highest correlation in LHF with GSSTF2 (0.81), due to the highest correlation in U_{10m} and especially Q_S–Q_{10m}. On the other hand, da Silva has the lowest correlation in LHF with GSSTF2 (0.51), due to the lowest correlation in U_{10m} and especially Q_S–Q_{10m}. The correlation is higher in the northern extratropical oceans than in the south for all variables, with the contrasts especially large for da Silva as a result of more missing ship observations in the south, consistent with the finding of Kubota et al. (2003). Over the tropical oceans, NCEP has a very low correlation in LHF with GSSTF2 (0.69). This is primarily a result of very low correlation in Q_S–Q_{10m}(0.27), which is close to that of da Silva (0.31) but is significantly smaller than that of HOAPS (0.81). This may be due to the lack of ship observations and the shortcoming of the cumulus and boundary parameterization used in NCEP. In short, our analyses suggest that the GSSTF2 LHF, surface air humidity, and winds are likely to be more realistic than the other three datasets analyzed, although those of GSSTF2 are still subject to regional biases.

6. CONCLUSIONS

The GSSTF2 daily LHF and input parameters compare reasonably well with those of nine collocated field experiments. Compared to the nine experiments, the GSSTF2 daily LHF has a bias of 0.8 W m^{-2}, a SD error of 35.8 W m^{-2}, and a correlation of 0.83. Daily wind speed has a bias of 0.36 m s^{-1}, a SD error of 1.38 m s^{-1}, and a correlation of 0.92. Daily surface air humidity has a bias of 0.67 g kg^{-1}, a SD error of 1.23 g kg^{-1}, and a correlation of 0.97. Assuming daily retrieval errors are independent, the SD errors for the monthly-mean LHF, wind speed, and surface air humidity reduce to 6.5 W m^{-2}, 0.25 m s^{-1}, and 0.22 g kg^{-1}, respectively.

The monthly LHF and input parameters (U_{10m}, Q_{10m}, and Q_S–Q_{10m}) of GSSTF2 over global oceans during 1992–93 are compared with those of HOAPS, NCEP, and da Silva. The large-scale patterns of the 2yr-mean fields for these variables are similar among these four datasets, but significant quantitative differences are found. Over the tropics, the HOAPS LHF is significantly smaller than GSSTF2 by ~31% (37 W m^{-2}), whereas the other two datasets are comparable to GSSTF2. This is because HOAPS has systematically smaller LHF than GSSTF2 in space, while the other two datasets have very large spatial variations of large positive and negative LHF differences with GSSTF2 which cancel to produce smaller regional-mean differences. The smallness of the HOAPS LHF is a result of smaller Q_S–Q_{10m} (0.7 g kg^{-1}) and U_{10m} (1.1 m s^{-1}), with the former mainly due to a larger Q_{10m} (by~1.1 g kg^{-1}). Over the northern (southern) extratropical oceans, the HOAPS LHF is smaller than GSSTF2 by 14 W m^{-2} (2 W m^{-2}). Averaged over the global oceans (60^oS–60^oN), the HOAPS LHF is smaller than GSSTF2 by 20 W m^{-2}. Our study and Brunke et al. (2002) suggest that the Q_{10m} of HOAPS and J-OFURO are likely to have larger positive biases than GSSTF2 in the tropical oceans.

In the equatorial Indian Ocean, SPCZ, ITCZ, the Kuroshio and Gulf Stream, and subtropics, the NCEP LHF is larger than GSSTF2, with the maximum difference up to 40 W m^{-2}. For the rest of the oceans, it is smaller than GSSTF2, with the maximum difference of ~60 W m^{-2} located in the dry tongue and trade wind region of the eastern South Pacific. The smaller NCEP LHF in the trade wind regions is a result of smaller Q_S–Q_{10m} and U_{10m}. For the equatorial Indian Ocean, SPCZ, and ITCZ, the larger NCEP LHF is because the effects of larger NCEP Q_S–Q_{10m} and moisture transfer coefficient overcompensate the effect of smaller U_{10m} on the LHF. The smaller NCEP LHF in the extratropical oceans is because the effect of smaller NCEP Q_S–Q_{10m} overcompensates the effects of larger U_{10m} and moisture transfer coefficient on the LHF. Averaged over the global oceans, the NCEP LHF is smaller than GSSTF2 by only ~3 W m^{-2} due to the large cancellation of local positive and negative differences with GSSTF2. The NCEP has extremely low temporal correlation (0.27) and large spatial variations of differences with GSSTF2 for Q_S–Q_{10m} in the tropics, which causes the low correlation for LHF. The very low temporal correlation of Q_S–Q_{10m} for NCEP, which is generally located in the data sparse tropics, is close to that of da Silva (0.31), but is significantly smaller than that of HOAPS (0.81).

The LHF difference of da Silva with GSSTF2 has small-scale structures, with its large-scale pattern somewhat similar to that of NCEP, but with larger magnitudes of difference. The da Silva is also found to have some nearby extreme large positive and negative LHF difference centers located in the data sparse regions. This feature is quite different than the more organized large-scale LHF difference patterns of HOAPS and NCEP (with GSSTF2). Due to the cancellation of these large local positive and negative differences, the regional-mean LHF of da Silva appears to be comparable to that of GSSTF2, except for the southern extratropical oceans with ~23% (22 W m^{-2}) smaller value than GSSTF2. This discrepancy is mainly due to a larger Q_{10m} (by ~1.2 g kg^{-1}) and is most likely due to the errors arising from extrapolating high values of Q_{10m} from low latitudes to the large data-void regions in the southern extratropical oceans. In addition, da Silva has extremely low temporal correlation and large differences with GSSTF2 for all variables in the southern extratropics, indicating that da Silva hardly produces a realistic variability in these variables. The temporal correlation is higher in the northern extratropics than in the south for all variables, with the contrast being especially large for da Silva as a result of more missing ship observations in the south, consistent with the finding of Kubota et al. (2003).

Based on comparison with high-quality flux observations, we conclude that the GSSTF2 LHF, surface air humidity, and winds are likely to be more realistic than the other three flux products examined, although those of GSSTF2 are still subject to regional biases. More high-quality observations covering wider areas of the global oceans (or more areas covering different climatic regimes) are vital to perform a more complete regional validation, to improve satellite retrieval, and to further confirm our conclusion. The GSSTF2 LHF, which is available at http://daac.gsfc.nasa.gov/CAMPAIGN_DOCS/hydrology/hd_gsstf2.0.html, is useful for climate studies.

REFERENCES

Brunke, M. A., X. Zeng, and S. Anderson, 2002: Uncertainties in sea surface turbulent flux algorithms and data sets. *J. Geophys. Res*., **107**, 10.1029/2001JC000992.

Brunke, M. A., C. W. Fairall, X. Zeng, L. Eymard, and J. A. Curry, 2003: Which bulk aerodynamic algorithms are least problematic in computing ocean surface turbulent fluxes? *J. Climate*, **16**, 619-635.

Chou, S.-H., R. M. Atlas, C.-L. Shie and J. Ardizzone, 1995: Estimates of surface humidity and latent heat fluxes over oceans from SSM/I data. *Mon. Wea. Rev*., **123**, 2405-2425.

Chou, S.-H., C.-L. Shie, R. M. Atlas and J. Ardizzone, 1997: Air-sea fluxes retrieved from Special Sensor Microwave Imager data. *J. Geophys. Res*., **102**, 12705-12726.

Chou, S.-H., W. Zhao, and M.-D. Chou, 2000: Surface heat budgets and sea surface temperature in the Pacific warm pool during TOGA COARE. *J. Climate,* **13**, 634-649.

Chou, S.-H., E. Nelkin, J. Ardizzone, R. M. Atlas, and C.-L. Shie, 2003: Surface turbulent heat and momentum fluxes over global oceans based on the Goddard satellite retrievals, version 2 (GSSTF2). *J. Climate*, **16**, 3256-3273.

Chou, S.-H., E. Nelkin, J. Ardizzone, and R. M. Atlas, 2004: A comparison of latent heat fluxes over global oceans for four flux products. J. Climate, accepted.

Curry, J. A., and coauthors, 2004: SEAFLUX. *Bull. Amer. Meteor. Soc*., 85, 409-424.

da Silva, A, C. C. Young and S. Levitus, 1994: Atlas of Surface Marine Data 1994 Vol. 1: Algorithms and Procedures. NOAA Atlas NESDIS 6, US Dept. of Commerce, NOAA, NESDIS, Washington, DC, 83 pp.

Fairall, C. W., A. B. White, J. B. Edson, and J. E. Hare, 1997: Integrated shipboard measurements of the marine boundary layer. *J. Atmos. Oceanic Technol.,* **14**, 338-359.

Fairall, C. W., E. F. Bradley, J. E. Hare, A. A. Grachev, and J. B. Edson, 2003: Bulk parameterization of air-sea fluxes: updates and verification for the COARE algorithm. *J. Climate*, **16**, 571-591.

Grassl, H., V. Jost, R. Kumar, J. Schulz, P. Bauer, and P. Schlussel, 2000: The Hamburg Ocean-Atmosphere Parameters and Fluxes from Satellite Data (HOAPS): A Climatological Atlas of Satellite-Derived Air-Sea-Interaction Parameters over the Oceans. Rep. 312, Max-Planck Institute for Meteorology, Hamburg, Germany, 130pp.

Josey, S. A., E. C. Kent and P. K. Taylor 1999: New insights into the ocean heat budget closure problem from analysis of the SOC air-sea flux climatology. *J. Climate*, **12**, 2856 - 2880.

Kalnay, E., and co-authors, 1996: The NCEP/NCAR 40-year reanalysis project. *Bull. Amer. Meteor. Soc*., **77**, 437-471.

Kent, E. C., and P. K. Taylor, 1997: Choice of a Beaufort equivalent scale. *J. Atmos. Oceanic Technol*., **14**, 228-242.

Kent, E. C., P. K. Taylor and P. G. Challenor, 2000: The characteristics of a sea surface temperature dataset smoothed by successive correction. *J. Climate*, **13**, 1845-1857.

Kubota, M., K. Ichikawa, N. Iwasaka, S. Kizu, M. Konda, and K. Kutsuwada, 2002: Japanese Ocean Flux Data Sets with Use of Remote Sensing Observations (J-OFURO) introducing J-OFURO. *J. Oceanogr.*, **58**, 213-215.

Kubota, M., A. Kano, H. Muramatsu and H. Tomita, 2003: Intercomparison of various surface latent heat flux fields. *J. Climate*, **16**, 670-678.

Large, W. G., and S. Pond, 1982: Sensible and latent heat flux measurements over the ocean. *J. Phys. Oceanogr*., **12**, 464–482.

Mears, C. A., D. Smith, and F.J. Wentz, 2001: Comparison of Special Sensor Microwave Imager and buoy-measured wind speeds from 1987 to 1997. *J. Geophys. Res*., **106**, 11719-11729.

Meissner, T., D. Smith, and F. J. Wentz, 2001: A 10-year intercomparison between collocated SSM/I oceanic surface wind speed retrievals and global analyses. *J. Geophys. Res*., **106**, 11731-11742.

Renfrew, I.A., G.W.K. Moore, P.S. Guest, and K. Bumke, 2002: A comparison of surface layer and surface turbulent flux observations over the Labrador Sea with ECMWF analyses and NCEP reanalyses. *J. Phys. Oceanogr*., **32**, 383-400.

Schulz, J., J. Meywerk, S. Ewald, and P. Schluessel, 1997: Evaluation of satellite-derived latent heat fluxes. *J. Climate*, **10**, 2782-2795.

Smith, S. D., 1988; Coefficients for sea surface wind stress, heat flux, and wind profiles as a function of wind speed and temperature. *J. Geophys. Res*., **93**, 2859-2874.

Smith, S. R., D. M. Legler, and K. V. Verzone, 2001: Quantifying uncertainties in NCEP reanalyses using high-quality research vessel observations. *J. Climate*. **14**, 4062-4072.

Wang, W., and M. J. McPhaden, 2001: What is the mean seasonal cycle of surface heat flux in the equatorial Pacific? *J. Geophys. Res*., **106**, 837-857.

Wentz, F. J., 1997: A well calibrated ocean algorithm for SSM/I. *J. Geophys. Res*., **102**, 8703-8718.

Zeng, X., M. Zhao, and R. E. Dickinson, 1998: Intercomparison of bulk aerodynamic algorithms for the computation of sea surface fluxes using TOGA COARE and TAO data. *J Climate*, **11**, 2628-2644.